Optics and Quantum Electronics

1. 5fs Pulses and Octave-Spanning Spectra from a Ti:sapphire Laser Oscillator

Sponsors
AFOSR

Project Staff
Richard Ell, Dr. Uwe Morgner, Professor Franz X. Kaertner, Professor James G. Fujimoto and Professor Erich P. Ippen

Pulses as short as 5 fs, with spectra extending from 600 to 1200 nm, have been generated directly with a Kerr-lens-modelocked (KLM) Ti:sapphire laser. A novel two-focus cavity is employed for added nonlinearity and double-chirped mirror pairs provide broadband controlled dispersion. The output spectra are the broadest ever generated directly from a laser oscillator.

The laser set-up is shown in Figure 1. Specially designed pairs of double-chirped mirrors [1] compensate for higher-order as well as second-order dispersion, and CaF_2 prisms permit dispersion adjustment. A 2.7-mm-thick Ti:sapphire crystal is pumped with about 4 W of cw 532 nm power. After modelocked operation is initiated by translating the prism P1, a steady state output power of about 120 mW can be obtained. Shorter pulses and additional spectral width are achieved with the added focus in a 2.4 mm thick plate of BK7 glass. Without this additional focus, saturation of the KLM effect in the Ti:sapphire crystal limits the amount of spectral broadening due to self-phase modulation as well. Our cavity is therefore designed to produce a short pulse and strong self-phase modulation but less of a Kerr-lensing effect in the second focus.

Pulses from the laser are recompressed externally by a sequence of double-chirped mirrors and CaF_2 prisms. They are then characterized with an interferometric autocorrelator using thin metal-coated beamsplitters and a thin, wedged KDP doubling crystal (10 – 40 ?m thick). Figure 2 shows the resulting autocorrelation along with the pulse spectrum (on linear and logarithmic scales). Also shown in Figure 2 are the envelope and phase of the pulse, derived with the use of a phase retrieval algorithm [2]. The intensity full-width at half-maximum is 5 fs. Curvature in the retrieved phase indicates that a further reduction in pulsewidth should be possible with a refined compensation scheme. The transform-limited width for the observed spectrum is 4.3 fs.

This work is carried out in collaboration with the Technical University of Karlsruhe.

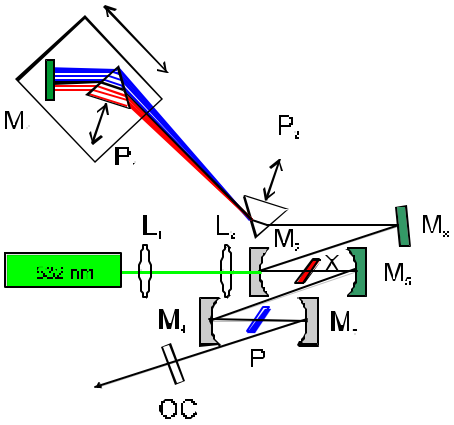

Figure 1: Schematic of 5 fs laser. Beam waists, in the Ti:sapphire crystal (X) and in a glass plate (P), facilitate both Kerr-lens modelocking and additional spectral broadening by self-phase modulation. Double-chirped mirrors, in addition to the CaF_2 prism pair, minimize net dispersion over an octave of bandwidth.

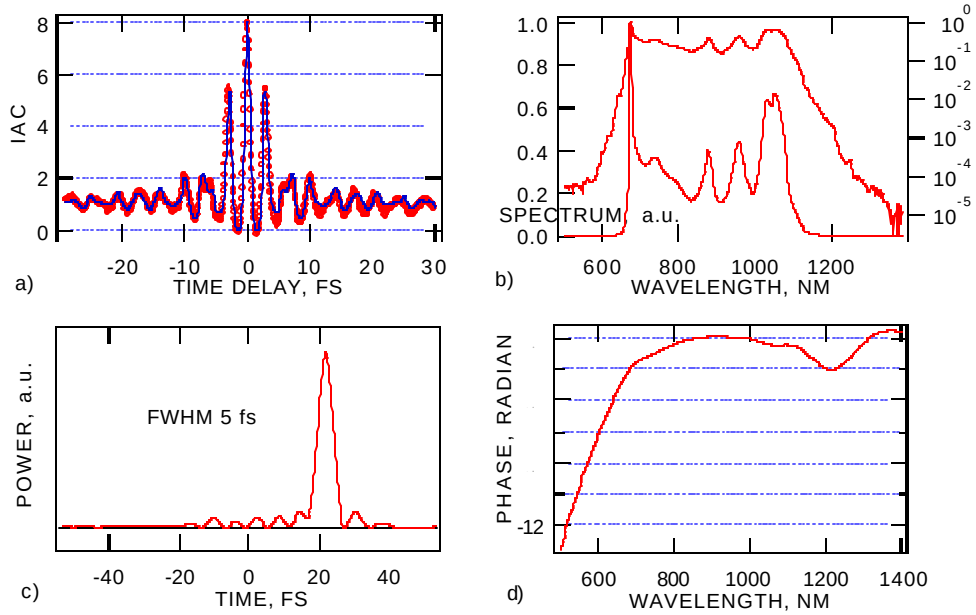

Figure 2: Interferometric autocorrelation of the 5 fs pulses (upper left); the spectrum in both linear and logarithmic scale (upper right); pulse envelope reconstruction (lower left); and recovered spectral phase (lower right).

References

1. U. Morgner et.al., Proceedings of CLEO'00, paper CThE5, Optical Society of America (2000)
2. A. Baltuska. A. Pugzlys. M. Pshenichnikov, D. Wiersma, B. Hoenders and H. Ferwerda, Ultrafast Optics, 221 (Ascona Th10)

Publications

1. F. X. Kaertner, U. Morgner, R. Ell, Ch. Jirauschek, G. Metzler, T. R. Schibli, Y. Chen, H. A. Haus, E.P. Ippen, J.G. Fujimoto, V. Scheuer, G. Angelow and T. Tschudi, "Challenges and limitations on generating few cycle laser pulses directly from oscillators," *Ultrafast Phenomena XII*, Springer Verlag, p. 51-55, 2000

2. R. Ell, U. Morgner, F. X. Kaertner, J. G. Fujimoto, E. P. Ippen, V. Scheuer, G. Angelow, T. Tschudi, M. J. Lederer, A. Boiko and B. Luther-Davies, "Generation of 5-fs pulses and octave-spanning spectra directly from a Ti:sapphire laser," *Opt. Lett.* 26, 273-5 (2001)

2. Nonlinear optics with phase-controlled pulses in the sub-two-cycle regime

Sponsors

AFOSR

Project Staff

Dr. Uwe Morgner, Richard Ell, Gerhart Metzler, Thomas Schibli, Professor F.X. Kaertner, Professor J.G. Fujimoto, Professor H.A. Haus and Professor E.P. Ippen

We have demonstrated a dependence of nonlinear optical frequency conversion on the phase of the optical carrier relative to the peak of the intensity envelope in ultrashort pulses. This is made possible by first generating sub-two cycle pulses with octave spanning spectra directly from a Ti:sapphire laser oscillator [1]. Detection of the carrier-envelope phase is then achieved by focusing the short pulses directly from the oscillator into a BBO-crystal. As a further example of nonlinear optics with such short pulses, the interference between second and third harmonic components was also demonstrated.

The carrier-envelope phase of pulses emerging from a laser is not known a priori, and it generally slips from pulse to pulse because the roundtrip phase delay in a laser is usually not the same as the roundtrip group delay. Nonlinear optical measurements that are sensitive to this carrier-envelope phase are not only interesting for ultrafast applications but can have a large impact on wavelength metrology as well. The slip rate of the phase determines the absolute positions of the frequency combs produced by mode-locked lasers, and these regularly spaced combs can be used to bridge the gap between atomic clock standards and optical frequencies [2,3].

One way to monitor the phase slip $d\phi/dt$ is to generate a second-harmonic pulse (with phase slipping at $2d\phi/dt$) and interfere it with the fundamental pulse. To obtain spectral overlap between the pulses requires at least an octave of fundamental spectrum. Previous workers [2,3] have accomplished this by using spectral broadening in optical fibers to obtain the octave. We have recently reported generating pulses that are sufficiently short, and broadband, directly from a laser oscillator.

Our experiment is illustrated in Figure 1. 5-fs pulses from our laser oscillator are focused into a BBO crystal for second-harmonic generation. At the output the interference signal between second-harmonic and fundamental is enhanced before detection by spectrally filtering the overlap regime (near 600 nm, since the fundamental spectrum spans from 600 nm to 1200 nm). The lower part of the figure shows the RF spectrum of the detected signal. The large spikes are harmonics of the roundtrip frequency; the two spikes in the middle are modulation sidebands shifted by the frequency of the phase slip. These modulation sidebands can be locked to a sub-harmonic of the roundtrip rate by feedback control of mirror position and tilt. Then phase-identical pulses can be selected at the sub-harmonic rate.

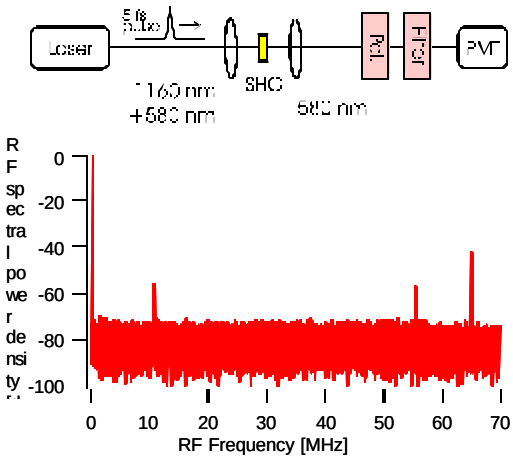

Figure 1: Experimental arrangement for the detection of second-harmonic and fundamental interference. The RF tones between the cavity rep-rate harmonics reveal the frequency of the phase slip.

Greater, phase-dependent, spectral overlap can be obtained between second and third harmonics. Our experiment for demonstrating this is shown in Figure 2. Third harmonics of the low frequency components in the pulse are generated by doubling and then summing. They are then combined with second harmonics of the high frequency components to produce the desired interference beat at d?/dt. In this case too, a spectral filter is used to isolate the proper spectral overlap to optimize the observed signal. Some improvement in the ratio of signal to background is evident. Clearly, with higher harmonic generation, spectral interference in the resulting harmonic spectrum will become increasingly prominent and dependent upon the carrier envelope phase of the initial pulse.

This work is carried out in collaboration with the Technical University of Karlsruhe.

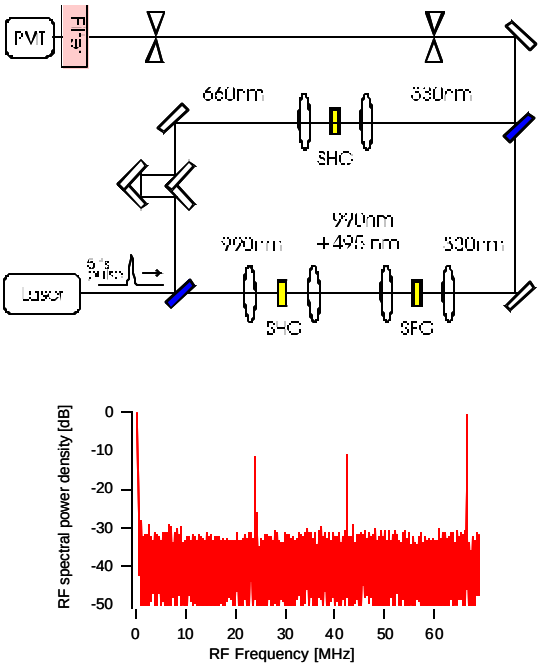

Figure 2: Experimental arrangement for observation of interference between second and third harmonic components. The RF tone left of center reveals the phase slip frequency; the tone right of center is given by the cavity roundtrip rate minus the slip frequency.

References

1. R. Ell, U. Morgner, F. X. Kaertner, J. G. Fujimoto, E. P. Ippen, V. Scheuer, G. Angelow, T. Tschudi, M. J. Lederer, A. Boiko and B. Luther-Davies, "Generation of 5-fs pulses and octave-spanning spectra directly from a Ti:sapphire laser," *Opt. Lett.* 26, 273-5 (2001)
2. D. Jones, S. Diddams, J. Ranka, A. Stentz, R. Windeler, J. Hall, and S. Cundiff, *Science* 288, 635-639 (2000).
3. A. Apolonski, A. Poppe, G. Tempea, C. Spielmann, T. Udem, R. Holzwarth, T. Haensch, and F. Krausz, *Phys. Rev. Lett.* 85, 740-743 (2000).

Publications

1. U. Morgner, R. Ell, G. Metzler, T. R. Schibli, F. X. Kaertner, J.G. Fujimoto, H. A. Haus and E. P. Ippen, " Nonlinear optics with phase-controlled pulses in the sub-two-cycle regime," *Phys. Rev. Lett*. in press.

3. Ultrafast Cr^{4+}:YAG Laser

Sponsors

AFOSR, NSF-MRSEC

Project Staff

Daniel Ripin, Dr. Christian Chudoba, Juliet Gopinath, Professor Franz Kärtner, Professor Erich P. Ippen

Several transition-metal doped materials are useful as ultrafast laser media because of their large gain bandwidths, convenient blue-shifted absorption spectra, and high nonlinear coefficients,

allowing for efficient Kerr-lens modelocking. Short pulsewidth sources obtained with such media are ideal for time-resolved studies of ultrafast phenomena and devices, as optical clocks with precise timing at the cavity repetition rate, and for ultra-high speed optical communications. The broad coherent bandwidth can be exploited for spectroscopy, to generate synchronized multi-wavelength optical sources, or for metrological optical frequency standards. Specific laser crystals are chosen for applications based on their material properties.

Cr^{4+}:YAG is a promising laser crystal with broad emission from 1350 nm to 1650 nm. This gain spectrum make this laser crystal ideal for optical telecommunications applications. In general, intracavity dispersion due to the laser crystal, prisms, and mirrors limits the bandwidth and pulsewidth of the emitted light pulses. The shortest pulses previously reported in the Cr^{4+}:YAG laser system are 43 fs pulses [1], which were generated in a laser cavity using two intracavity fused silica prisms to compensate the group delay dispersion (GDD) from the Cr^{4+}:YAG crystal. It is thought that third order dispersion (TOD) limits the pulsewidth in this system [2].

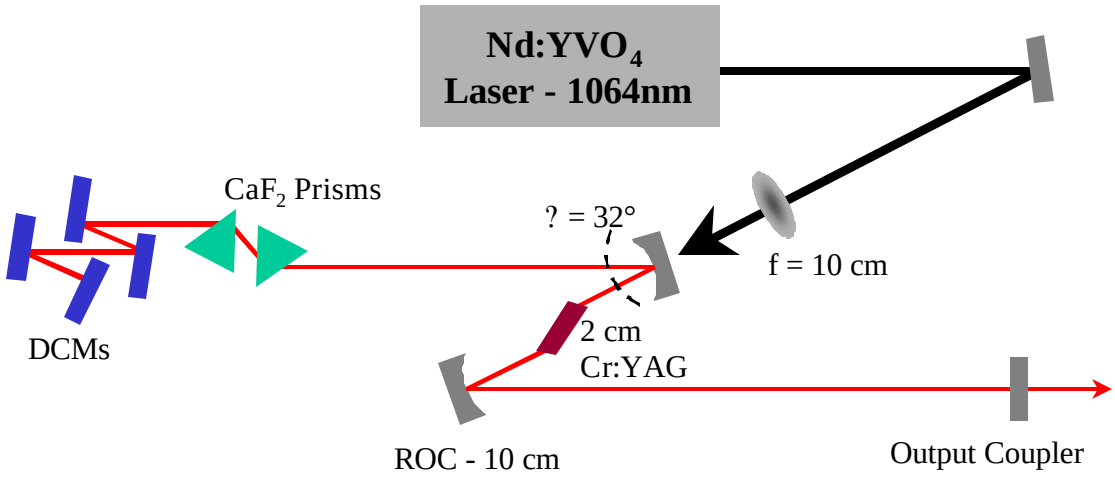

Fig. 1. A schematic of the Cr^{4+}:YAG laser cavity. A 2 cm Cr^{4+}:YAG crystal was placed inside a Z-fold cavity between 2 folding mirrors with a 10 cm radius-of-curvature. The laser is optically pumped by a Nd:YVO_4 laser emitting cw light at 1064 nm. The cavity is designed to have seven round-trip bounces off double chirped mirrors (DCMs) for dispersion compensation. Two CaF_2 prisms provide fine tuning of the cavity dispersion.

We have demonstrated the generation of 36 fs pulses from a dispersion compensated Cr^{4+}:YAG laser. Shorter pulse widths were obtained by reducing TOD. A schematic of the laser cavity is shown in Figure 1. A 2 cm Cr^{4+}:YAG crystal was placed inside a Z-fold cavity designed to maximize Kerr-lens modelocking while simultaneously compensating for astigmatism. The laser is optically pumped by a Nd:YVO_4 laser emitting cw light at 1064 nm. Seven round-trip bounces off Double chirped mirrors (DCMs) are used to simultaneously compensate GDD and TOD; CaF_2 prisms are used optimized the pulsewidth by fine tuning the intracavity dispersion. A plot of the calculated cavity dispersion is shown in Figure 2. By purging the laser cavity with N_2 gas to eliminate water absorption, it was possible to generate optical pulses with a center wavelength of 1480 nm, and significant spectrum below 1500 nm.

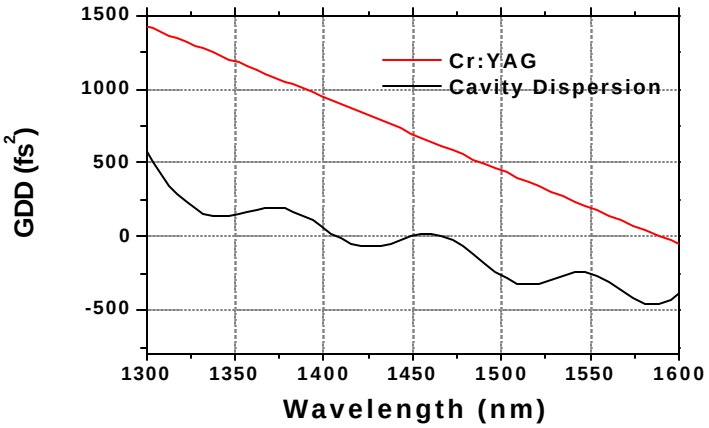

Fig. 2. Plot of the total cavity dispersion. The dispersion through a 2 cm Cr^{4+}:YAG crystal (roundtrip) is also plotted.

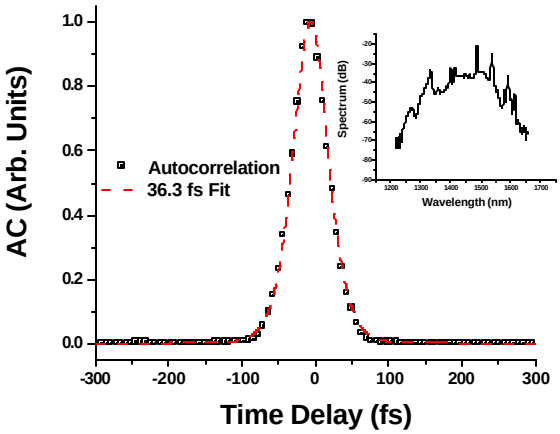

Fig. 3. Autocorrelation of 36 fs Cr^{4+}:YAG laser pulses. The corresponding pulse spectrum is inset.

The pulse width was measured to be 36 fs with a background-free autocorrelation and is shown in Figure 3. The corresponding pulse spectrum is inset and has a full width at half maximum of ~ 100 nm.

References

1. Y. P. Tong, P. M. W. French, J. R. Taylor, J. O. Fujimoto, "All-solid-state femtosecond sources in the near infrared"; *Opt. Comm.* 136: 235-238 (1997).

2. Tatsuya Tomaru and Hrvoje Petek, "Effect of third-order dispersion on the phases of solitonlike Cr^{4+}:YAG-laser pulses characterized by the second-harmonic generation frequency-resolved optical gating method"; J. *Opt. Soc. Am. B*, 18: 388-393 (2001).

4. Noise Studies in Active Harmonically Modelocked Fiber Lasers

Sponsors
DARPA, AFOSR

Project Staff
Matthew E. Grein, Dr. Yijiang Chen, Professor Erich Ippen, Professor Hermann A. Haus

The low-timing jitter performance of actively modelocked fiber lasers makes them suitable candidates as optical clocks for precision, high-speed optical analog-to-digital converters. Much of the low-noise performance—compared with semiconductor lasers—arises due to the long upper-state lifetime of the rare-earth dopants in the amplifier that integrates over gain dynamics.

The active modelocking of fiber lasers is achieved with two types of modelockers: amplitude (AM) and phase (PM) modulation, yielding similar performance with respect to pulse shaping and stability. In the formalized treatment of jitter in actively modelocked lasers [1], the theory is developed for amplitude modulation (AM), and the jitter is expressed as excitations (driven by noise) that are damped by characteristic time constants that describe the laser's dynamic response to noise. The time constants are related to the laser parameters, such as modulation depth, filtering, and group-velocity dispersion (GVD). The purpose of our study is to develop a stable, active, harmonically modelocked fiber laser operating at 10 GHz producing picosecond pulses with low timing jitter, and to understand its quantum-limited performance.

We have developed two actively modelocked fiber laser configurations producing pulses at 10 GHz. The first laser setup--shown in Fig. 1—employs a ring geometry with polarization-maintaining fibers. An isolator ensures unidirectional lasing, an erbium-doped amplifier provides gain, and the laser can be actively modelocked using either amplitude or phase modulation. The RF synthesizer is set to the frequency of the cavity harmonic closest to 10 GHz for active modelocking.

The second laser setup—shown in Fig. 2--is arranged in a sigma-type configuration in which the linear portion is composed of non-polarization-maintaining elements. The amplifying medium is an Er:Yb double-clad fiber side-pumped with a multimode 980 laser diode. The sigma laser works as follows: a pulse exiting the polarizing beam splitter (PBS) from the ring depolarizes due to environmentally-induced birefringence in the linear segment. A faraday rotator at the end of the linear segment ensures that the backward-propagating pulse travels along the orthogonal polarization axis with respect to the forward-traveling pulse. In this way, the polarization effects in the forward and backward propagating directions are averaged out so that the pulse arrives at the polarization beam splitter again with a linear polarization.

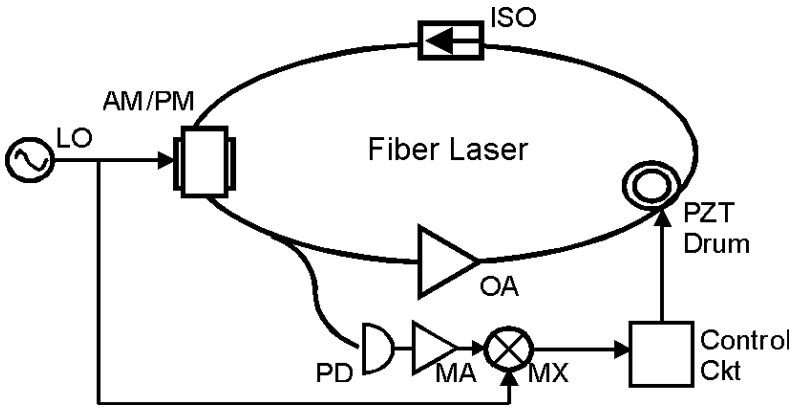

Figure 1: Laser configuration; the abbreviations are ISO isolator, AM/PM amplitude or phase modulator, PZT piezo-electric, LO local oscillator, OA optical amplifier, PD photodiode, MA microwave preamplifier, MX mixer, CKT circuit power

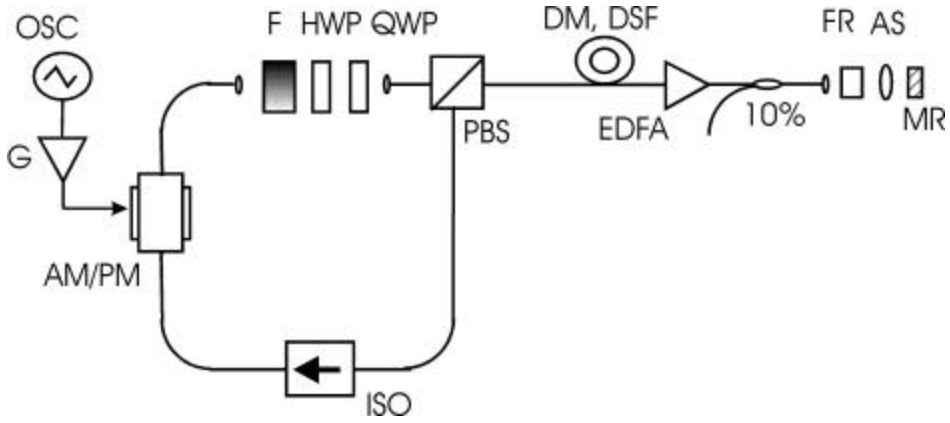

Figure 2: Sigma laser configuration

The pulses derived from both configurations vary from between 900 fs and 2 ps, depending on the filtering and pump power, and are very close to the transform-limit for hyperbolic secant pulse shapes. The typical suppression of supermodes in the RF spectrum is greater than 65 dB, indicative of excellent laser stability.

To keep both lasers actively modelocked, we employ active stabilization of the cavity length compared to a reference oscillator (shown explicitly in Fig. 1). The phase of the fundamental RF tone of the detected laser signal (10 GHz) is compared with that of an external reference with simple homodyne detection. Any phase error generates a voltage that is integrated and amplified to drive a fiber-wound PZT that changes the length of the laser cavity, completing a phase-locked feedback loop that ensures stable active modelocking in the presence of environmental perturbations.

The pulse quality is not very sensitive to modulation with either AM or PM; however, we expect that the jitter should be very different. In contrast to the case of AM, pulse timing is not restored directly by PM. Mistimed pulses first experience a shift in frequency that converts to retiming through group-velocity dispersion (GVD). Upon successive round trips, the accumulated frequency shifts are damped out by filtering. Our preliminary results indicate that the minimum quantum-limited jitter for AM requires dispersion management in which the local dispersion

swings between anomalous and normal, but the net dispersion of the cavity is near zero. This reduces the jitter due to frequency fluctuations while enhancing the pulse energy. We have shown theoretically that for AM, the quantum-limited jitter is proportional to the square of GVD. For PM, however the quantum-limited timing jitter grows linearly with GVD for large GVD and inversely proportional to GVD for small GVD --these cases (for fixed pulse energy) are shown in Fig. 3 For PM, the minimum jitter requires an optimum dispersion because large dispersion increases the timing recovery from noise that comes from timing fluctuations, but dispersion also increases the noise that comes from frequency shifts via the Gordon-Haus effect.

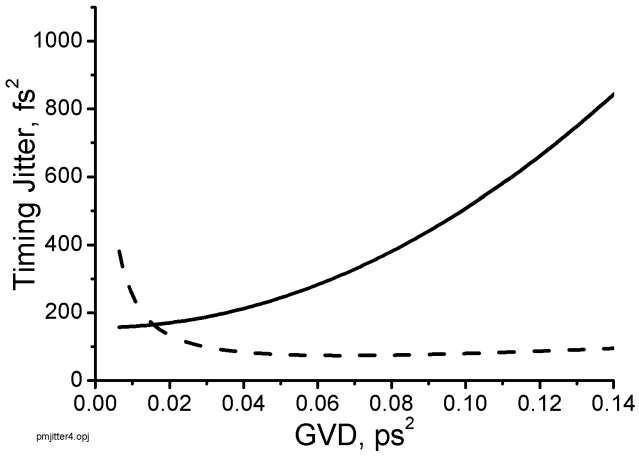

Figure 3: Quantum-limited jitter for amplitude (solid line) and phase (dotted line) modulation for fixed pulse energy.

References

1. H. A. Haus and A. Mecozzi, "Noise of modelocked lasers", *IEEE J. Quantum Electron.* 29: 983 (1993).

Publications

1. M. E. Grein, L. A. Jiang, Y. Chen, H A. Haus, and E. P. Ippen, "Timing restoration dynamics in an actively mode-locked fiber ring laser", *Optics Lett.* 24: 1687-1689 (1999).

2. M. E. Grein, L. A. Jiang, Y. Chen, H A. Haus, and E. P. Ippen, "A study of the of the dynamics governing timing restoration in the actively modelocked soliton laser," paper presented at the 1999 Conference on Lasers and Electro-Optics, Baltimore, Maryland, May 23-28, 1999.

3. M. E. Grein, L. A. Jiang, Y. Chen, H A. Haus, and E. P. Ippen, "The quantum limit of the timing jitter in actively mode-locked soliton fiber lasers", to be submitted to *IEEE J. Quant. Electron.*

4. M. E. Grein, Y. Chen, H A. Haus, and E. P. Ippen, "The quantum limit of the timing jitter in actively mode-locked soliton fiber lasers," paper to be presented at the 2001 Conference on Lasers and Electro-Optics, Baltimore, Maryland, May 6-11, 2001.

5. Stabilization of Active, Harmonically Modelocked Fiber Lasers using Two-Photon Absorbers

Sponsors
DARPA, AFOSR

Project Staff
Matthew E. Grein, Erik R. Thoen, Elizabeth M. Koontz, Professor Erich P. Ippen, Professor Hermann A. Haus, Professor Leslie A. Kolodziejski

Active harmonically mode-locked fiber lasers producing picosecond pulses at gigahertz repetition rates for communications and precision optical sampling require a mechanism to equalize pulse energies to prevent amplitude fluctuations and pulse dropouts[1-4]. Recently, it was shown that two-photon absorption (TPA) can limit the peak intensity of Q-switched mode-locking and enhance the stability of continuous-wave mode-locking [5-6]. In this paper, it is shown that a semiconductor mirror providing TPA in a harmonically mode-locked fiber laser introduces a fast intensity-dependent loss that can equalize pulse energies and reduce pulse dropouts.

Figure 1 shows a ~ 47 m active harmonically mode-locked fiber laser operating at 2 GHz. The average group-velocity dispersion is ~ 6 ps/nm/km (anomalous). The fibers are polarization maintaining to eliminate additive-pulse limiting effects. A circulator incorporates a mirror in the ring cavity. An aspheric lens is used to produce a small spot size (~ $5x10^{-8}$ cm^2) on the mirror. To test the laser operation without TPA, a dielectric mirror (> 99.9% reflectivity at 1.55 ?m) was used in this position. Autocorrelations yielded transform-limited 1.8 ps pulses at 1.555 ?m. The RF spectrum exhibited 25 dB supermode suppression, as shown in Fig. 2a, indicative of pulse dropouts. Fig. 2b shows a digital oscilloscope scan over a long time scale (tens of ns) as compared to the repetition rate (500 ps), verifying that pulses are missing. Note that individual pulses are not resolved due to the limited resolution of the oscilloscope.

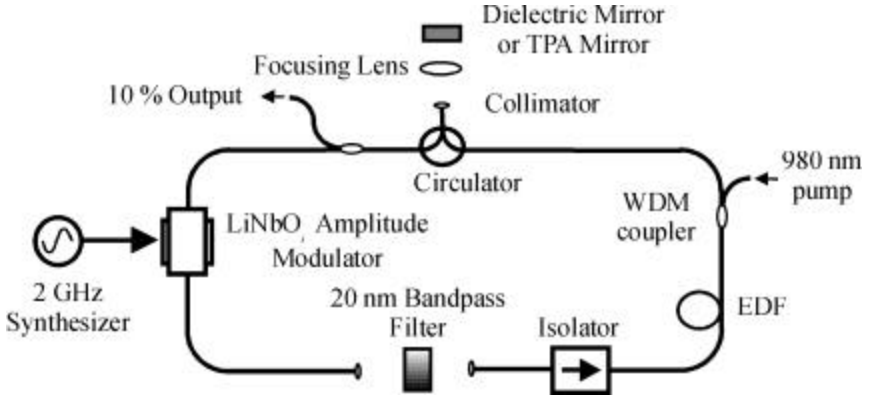

Figure 1: Laser setup; all fibers are polarization maintaining.

The dielectric mirror was replaced by a TPA mirror, and with the average power held constant, the laser produced pulses of similar duration. The TPA mirror consists of a ~5.1 ?m InP layer deposited via gas source molecular beam epitaxy onto a 22 period GaAs/AlAs distributed Bragg reflector (>99% reflectivity at 1.55 ?m). A dielectric antireflection coating was deposited on the TPA mirror. TPA introduces an instantaneously greater loss for higher peak intensity, which suppresses amplitude fluctuations and pulse dropouts by favoring a filled pulse train of low-intensity pulses over a partially filled pulse train of high-intensity pulses. The supermode suppression shown in Fig. 3a was enhanced by 30 dB (compared with Fig. 2a), and the corresponding oscilloscope trace in Fig. 3b reveals the absence of pulse dropouts. Based on

nonlinear reflectivity measurements of a similar structure and the incident peak intensity, the nonlinear loss of the TPA mirror was estimated to be between 0.5 and 1%. To verify the intensity dependence of the TPA effect, the peak intensity on the TPA mirror was lowered dramatically by removing the focusing lens (spot size ~ 9.5×10^{-3} cm^2), yielding results similar to those of Fig. 2.

Some of the novel features of TPA-assisted harmonic mode-locking are the enabled operation of environmentally stable, short laser cavities; the potential for specific tailoring of semiconductor materials and waveguide structures for optimum performance and integration; and laser operation even in the non-soliton regime.

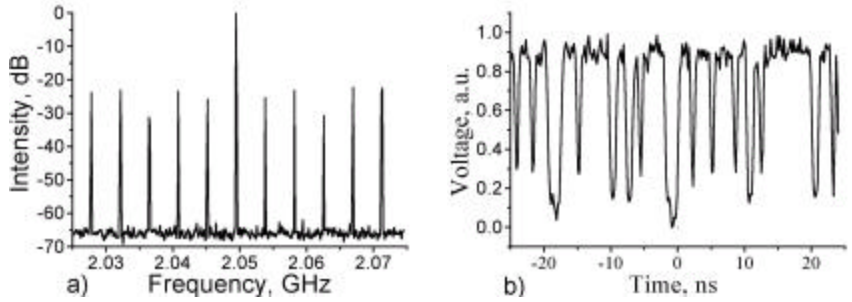

Figure 2: Laser output without the TPA mirror. a) RF power spectrum, 3 kHz resolution bandwidth, and b) Digitizing oscilloscope trace.

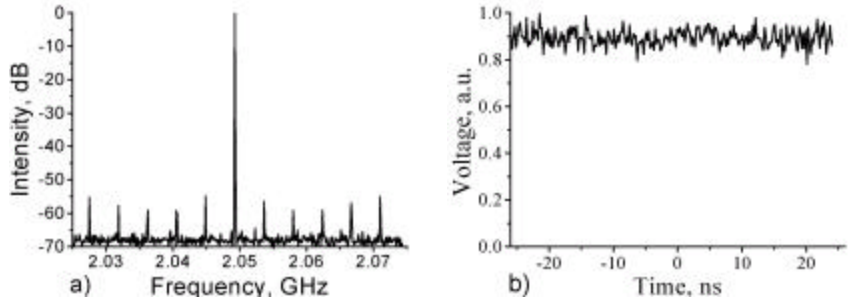

Figure 3: Laser output with the TPA mirror and focusing lens. a) RF power spectrum, 3 kHz resolution bandwidth, and b) Digitizing oscilloscope trace.

References

1. X. Shan and D. M. Spirit, "Novel method to suppress noise in harmonically modelocked erbium fibre lasers", *Electron. Lett.* 29: 979 (1993).

2. G. T. Harvey and L. F. Mollenauer, "Harmonically mode-locked fiber ring laser with an internal Fabry-Perot stabilizer for soliton transmission", *Opt. Lett.* 18:107 (1993).

3. C. R. Doerr, H. A. Haus, E. P. Ippen, M. Shirasaki, and K. Tamura, "Additive-pulse limiting", *Opt. Lett.* 19: 31 (1994).

4. M. Nakazawa, K. Tamura, and E. Yoshida, "Supermode noise suppression in a harmonically modelocked fibre laser by self-phase modulation and spectral filtering," Electron. Lett. 32: 461 (1996).

Publications

1. E. R. Thoen, Grein, M. E., E. M. Koontz, H. A. Haus, L. A. Kolodziejski, and E. P. Ippen, "Stabilization of an active harmonically mode-locked fiber laser using two-photon absorption", *Opt. Lett.* 25: 948-950 (2000).

2. E. R. Thoen, E. M. Koontz, M. Joschko, P. Langlois, T. R. Schibli, F. X. Kartner, E. P. Ippen, and L. A. Kolodziejski, *Appl. Phys. Lett.* 74: 3927 (1999).

3. M. E. Grein, E. R. Thoen, E. M. Koontz, H. A. Haus, L. A. Kolodziejski, and E. P. Ippen, "Stabilization of an active harmonically mode-locked fiber laser using two-photon absorption", Paper presented at the 2000 Conference on Lasers and Electro-Optics, San Francisco, California, May 7-12, 2000.

Thesis

E. R. Thoen, *Development of Ultrashort Pulse Fiber Lasers for Optical Communication Utilizing Semiconductor Devices*, Massachusetts Institute of Technology, June 2000.

6. Noise Studies in Passively Modelocked, Regeneratively Synchronized Fiber Lasers

Sponsors

DARPA, AFOSR, ONR

Project Staff

Charles X. Yu, Matthew E. Grein, Professor Erich Ippen, Professor Hermann A. Haus

Erbium-doped fiber lasers are attractive as high repetition rate sources for many applications, e.g. telecommunications and optical sampling. Actively modelocked lasers can provide trains of low-noise pulses at GHz repetition rates, but even with soliton shortening can not achieve pulse widths much shorter than a picosecond. While passively modelocked sources can produce pulses as short as a few hundred femtoseconds, they have not shown to produce stable, low noise trains of pulse at GHz repetition rates. We recently demonstrated that a passively modelocked fiber laser operating at a MHz repetition rate can be regeneratively synchronized using a phase modulator and microwave clock to produce a train of subpicosecond pulses at GHz repetition rates. The purpose of this study is to study the timing jitter of that source.

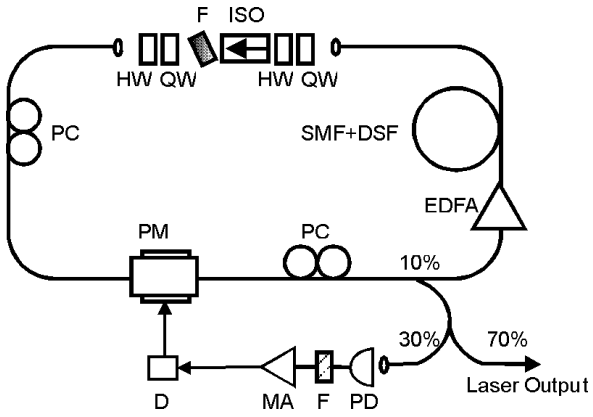

Figure 1: Regeneratively synchronized, passively modelocked fiber laser setup. The abbreviations are HW half-wave plate, QW quarter-wave plate, PC polarization controller, PM phase modulator, EDFA erbium-doped fiber amplifier, SMF single-mode fiber, DSF dispersion-shifted fiber, PD photodiode, F filter, MA microwave amplifier, D delay.

The laser schematic is shown in Fig. 1. The waveplates and the polarization controllers provide polarization APM. The output from the 10% coupler is 10 mW and 30% of the output is detected, filtered, amplifier, and phase-shifted to drive the phase modulator. The cavity dispersion is 8 ps/nm/km. The amplitude and timing jitter of the laser is measured with a 12 GHz detector and an 8 GHz RF spectrum analyzer—the first and seventh harmonic are shown in Fig. 2. One part of the amplitude noise structure extends to 300 kHz—this part is constant around all of the laser harmonics. Its overall magnitude is 0.04% via numerical integration (the discreet spikes on the harmonic spaced at 120 Hz are due to mechanical vibrations and removed when calculating the jitter). There is another narrowband noise structure that extends to 250 kHz. Part of this structure may be due to the local oscillator noise of the spectrum analyzer and pump noise. The upper limit of this noise structure is 0.1%. This amplitude noise is lower than actively modelocked lasers [1-3] but comparable to that of passively modelocked fiber lasers [4]. The timing jitter is 35 fs for frequencies above 100 Hz (lower than the 90 fs reported in [2]) and 86 fs close to the carrier. Our model for the jitter shown in Fig. 2 overestimates the close-in jitter below 200 Hz, but agrees well with the jitter in the wings. This is an indication that the jitter at frequencies greater than 200 Hz is dominated by white noise and suggests that the timing jitter for frequencies above 200 Hz is quantum limited.

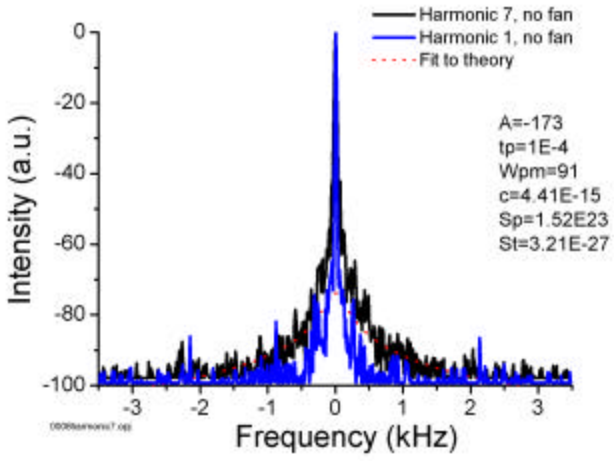

Figure 2: RF spectrum of the laser in Fig. 6. Solid black line, harmonic one; Solid blue, harmonic 7; Dashed red line, fit to theory. The fitting parameters are also shown.

References

1. E. Yoshida and M. Nakazawa, “Measurement of the timing jitter and pulse energy fluctuation of a PLL regeneratively modelocked fiber laser,” *IEEE Photon. Tech. Lett.* 11: 548 (1999).

2. K. Gupta, D. Novak, and H. Liu, “Noise characterization of a regeneratively modelocked fiber ring laser,” *IEEE J. Quant. Electron.* 36: 70 (2000).

3. T. Clark, T. Carruthers, P. Matthews, and I. Duling, “Phase noise measurements of ultrastable 10 GHz harmonically modelocked fiber laser,” *Electron. Lett*. 35: 720 (1999).

4. S. Namiki, C. X. Yu, and H. A. Haus, “Observation of nearly quantum-limited timing jitter in an P-APM all fiber ring laser,” *J. Opt. Soc. Am. B* 13: 2817 (1996).

Publications

1. M. Margalit, C. X. Yu, E. P. Ippen, and H. A. Haus, “Harmonic mode-locking using regenerative phase modulation,” *IEEE Photon. Tech. Lett.* 10: 337 (1998).

2. H. A. Haus, C. X. Yu, M. E. Grein, and E. P. Ippen, “The timing jitter of a regenerative mode-locked fiber ring laser”, *Quantum Electronics and Femtosecond Optics*, Memo 102.

3. C. X. Yu, M. E. Grein, H. A. Haus, and E. P. Ippen, “Noise of a regeneratively synchronized GHz passively modelocked fiber laser”, *Conference on Lasers and Electro-Optics Europe*, Nice, France, May 7-12, 2000, paper CTuK106.

7. Noise in Modelocked Laser Diodes

Sponsor

DARPA

Project Staff

Leaf A. Jiang, Mathew E. Grein, Professor Erich P. Ippen, Professor Hermann A. Haus

Analytical expressions for the amplitude, frequency, timing, and carrier phase noise of modelocked laser diodes were derived. It was found both experimentally and theoretically that carrier dynamics contribute significantly to the total noise of mode-locked laser diodes (MLLDs). In addition, optical cross-correlations more accurately measure timing jitter than RF techniques.

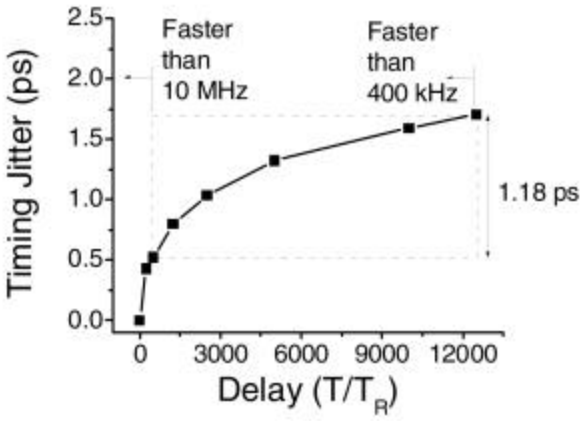

Figure 1: Pulse-to-clock RMS timing jitter is plotted as a function of delay for the actively MLLD.

Noise limits performance in communications and in high-speed optical sampling [1]. In communications, noise bounds the bitrate-distance product and ultimately limits the receiver sensitivity. The noise of a MLLD is very different from that of other laser systems, such as fiber lasers, Neodymium:YAG lasers, Ti:Sapphire lasers, and other lasers with slow gain dynamics. The difference stems from the fact that the carrier lifetime is very short for MLLDs and hence effects of the gain fluctuations on the timing of the pulses are very important on a round-trip time scale. We can understand the effect of carrier fluctuations on timing jitter from two physical pictures: (1) Fluctuations in gain and pulse energies affect the saturation dynamics which causes the front of the pulse to experience more gain than the back of the pulse, effectively moving the pulse forward. (2) Variations of the total gain cause variations in the refractive index which also changes the round-trip time of the cavity. Fig. 1 shows the measured pulse-to-pulse timing jitter as a function of delay, which is due to carrier contributions, spontaneous emission, shot noise of the carriers and modelocker noise. For our actively MLLD, the modelocker contributes the most noise and the carrier shot noise contribution makes up a large portion of the total quantum noise. Analytical solutions for the noise variance have been found and correspond well to experimental measurements. As expected theoretically, the timing jitter increases as the square root of the delay and starts to saturate at long delays since the active modulation pushes the pulses back into their time-slot.

Laser noise measurements typically involve RF mixing techniques that can often only resolve noise fluctuations less than several tens of MHz [2]. Since the noise of modelocked laser diodes contains high frequency components around the relaxation oscillation frequency of the laser, these techniques are not appropriate to characterize faster fluctuations of the modelocked laser on a pulse-to-pulse time scale. Therefore, we have used optical cross-correlations to measure the high frequency noise which has previously been ignored but is very important for high-speed optical analog-to-digital converters. The setup for the optical cross-correlations is shown in Fig. 2 and a sample measurement is shown in Fig. 3. The broadening of the cross-correlation is due to timing jitter. Dispersion of the delay-line does not affect our measurement since we calibrate its effect by placing the delay line before the optical correlator and autocorrelating the dispersed pulses. Therefore, we can extract the broadening of the cross-correlation due to timing jitter alone. By taking autocorrelations for different delays, we can reconstruct the plot in Fig. 1, which shows the contribution of the low and high frequency noise to the total jitter. The bandwidth of the noise is inversely related to the pulse-to-pulse delay. This is the first time that attention has been brought to the high frequency noise of these modelocked lasers, and has been found to contribute up to half the total noise power.

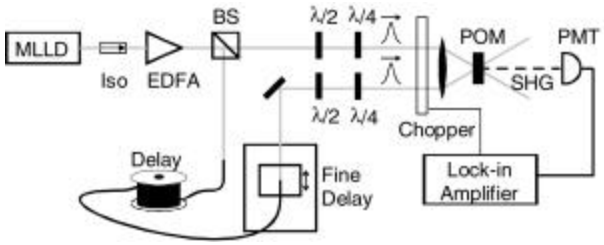

Figure 2: The experimental setup used to measure timing jitter.

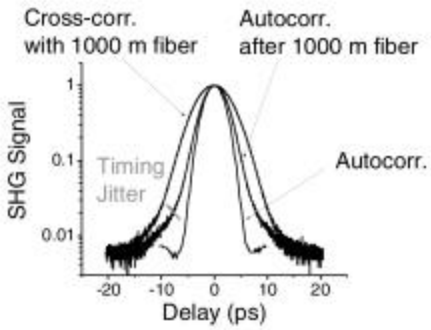

Figure 3: Optical correlations with 1000~m fiber delay. The second harmonic generation is plotted as a function of fine delay.

References

1. P. W. Juodawlkis, J. C. Twichell, J. L. Wasserman, and R. C. Williamson, "Measurement of mode-locked laser timing jitter using phase-encoded optical sampling," CLEO May 2000, OSA, San Francisco

2. D. von der Linde, "Characterization of noise in continuously operating mode-locked lasers," *Appl. Phys. B*, 39: 201-217 (1986).

Publications

1. L. A. Jiang, M. E. Grein, E. P. Ippen, and H. A. Haus, "Noise of Modelocked Laser Diodes." ISLC '00. ThB5. Laser Dynamics.

8. Full-pulse Characterization Using Autocorrelations and Genetic Algorithm

Sponsor

DARPA

Project Staff

Leaf A. Jiang, Mathew E. Grein, Professor Erich P. Ippen, Professor Hermann A. Haus

We have demonstrated a technique for extracting the amplitude and chirp of optical pulses, from autocorrelation measurements of pulses after propagation through different lengths of fiber, by using a genetic algorithm. Nonlinearities in the fiber are taken into account and computation time is greatly reduced by encoding the chromosomes with a Hermite-Gaussian expansion.

The recovery of a pulse's amplitude and chirp from intensity autocorrelations after different spans of fiber is a well-known method [1]. If the propagation through the fiber is linear, i.e. is only dispersive, the phase and amplitude can be recovered by the use of a phase-retrieval algorithm, much like FROG [2]. The parameter range for which this can be done is rather limited, since high powers are needed to obtain good nonlinear conversion in the autocorrelator but also result in unwanted self-phase modulation in the fiber. This can either be due to the use of short pulses with high peak powers, or amplified picosecond pulses (as in the case of communication systems). There is an inherent trade-off between the amount of second harmonic generation in the autocorrelator and nonlinear Kerr effect in the fiber. Since nonlinear propagation is rather complicated and the evolution of a pulse cannot simply be written as a function of the known values, genetic algorithms lend themselves well to pulse-recovery since they deal directly with the solution space, while conveniently ignoring the details of the problem (i.e. don't need information about derivatives, etc.). In addition, genetic algorithms readily take advantage of parallel computing and have already shown that there can be improved performance in recovering pulses from spectrograms [3] over that of other deterministic optimization schemes [4].

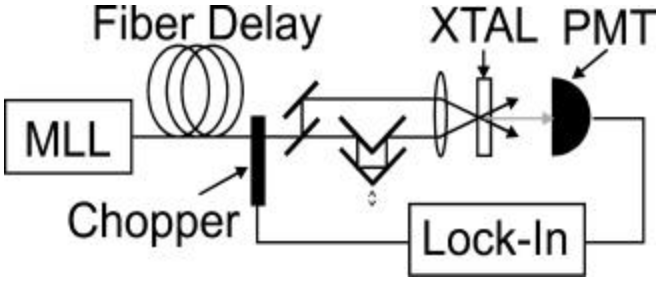

Figure 1: The experimental setup showing a non-colinear intensity autocorrelator. The nonlinear crystal used was POM. The sum generation was detected on a photomultiplier tube (PMT). Chopping was done to increase the signal-to-noise ratio.

The experimental setup used to measure the amplitude and phase (or chirp) of a pulse is shown in Fig. 1. In our experiments, a 5 GHz actively mode-locked external cavity 1.5 ?m laser diode was used as the source. The pulses had a full-width at half intensity maximum (FWHM) of approximately 3 ps and were amplified to 15 dBm with an erbium-doped fiber amplifier to obtain an autocorrelation trace with a good signal-to-noise ratio. These pulses were autocorrelated after 0, 10, 20, 50, 100, 200, 400, and 500 meters of Corning LEAF fiber that has a dispersion of 4 ps/nm/km at 1540 nm and an effective area of 72 $?m^2$. Using seven fiber segments reduces the possibility of non-unique solutions. For the experimental data, all eight autocorrelations corresponding to the aforementioned fiber delays were used in the fitness tests. Incorporating nonlinear propagation in the pulse-recovery algorithm is important since the wings in the autocorrelation due to the Kerr nonlinearity in the fiber are incorrectly interpreted as an echo pulse when linear propagation is used. Indeed, when we run the genetic algorithm to recover the input pulse shape, an echo pulse appears, as can be seen in Fig. 2.

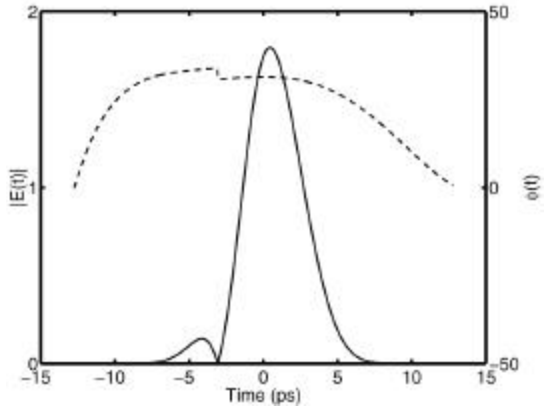

Figure 2: Recovered electric-field of the input pulse assuming linear propagation in genetic algorithm. Solid line is the amplitude and the dotted line.

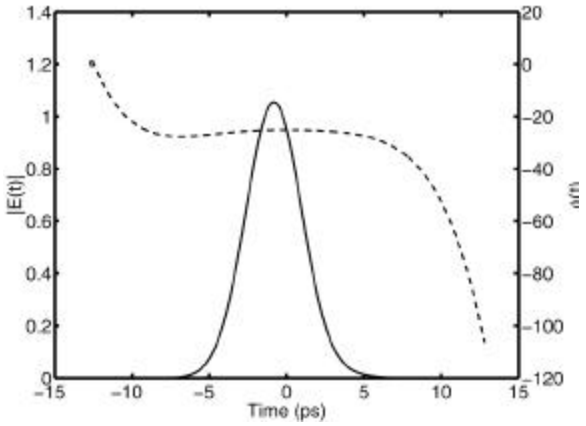

Figure 3: Recovered electric-field of the input pulse taking into account nonlinear propagation in the genetic algorithm.

Using nonlinear propagation, which is easy to incorporate into the genetic algorithm code, we obtain a more accurate reconstruction of the input pulse amplitude and phase. Fig. 3 shows the reconstructed amplitude and phase of the input pulse using the same data, but here we also take into account the nonlinear effects of the fiber by including the Kerr nonlinearity in our pulse propagation code, and hence obtain a more accurate reconstruction of the input pulse.

The method of encoding the electric-field into a chromosome is a key issue when using genetic algorithms. An encoding that does not suit a particular problem can greatly increase the computation time. In our algorithm, we chose to represent the electric-field as a sum of Hermite-Gaussian functions. Each chromosome is composed of the pulse width, Hermite-Gaussian coefficients, and chirp coefficients. We typically found that only 13 to 20 genes were sufficient for representing the pulse shapes shown in this paper. Hermite-Gaussian encoding has significant advantages over real number "sampled E-field" encoding [3]. For example, when we used the "sampled E-field" genes, we were not able to recover the input pulse after 100 generations. On the other hand, when we used the Hermite-Gaussian genes, the input pulse converged to that shown in Fig. 3 after only ~20 generations.

To test the algorithm, the troublesome cases of chirped double pulses with and without noise were tried numerically. The autocorrelations of the pulses after propagation through 0, 10, 20, 50, 100, 400, and 500 m of LEAF fiber were simulated. Using these autocorrelations for the

fitness test, we were able to accurately reconstruct our original input pulses using our genetic algorithm. The double pulse was a sum of two chirped hyperbolic secant pulses each with a FWHM of 1 ps and separated by 2.5 ps. It was found that the chromosomes converged to the correct answer for many different mutation strengths, crossover probabilities, and selection types. Fig. 4 shows the recovered pulses for an initial population of 100 chromosomes after 100 generations. Each chromosome had 20 genes and was initialized to within 30% of the exact answer. The amplitude and phase matches well over the region which the pulse has significant energy and the fitness of the chromosomes improves with each generation.

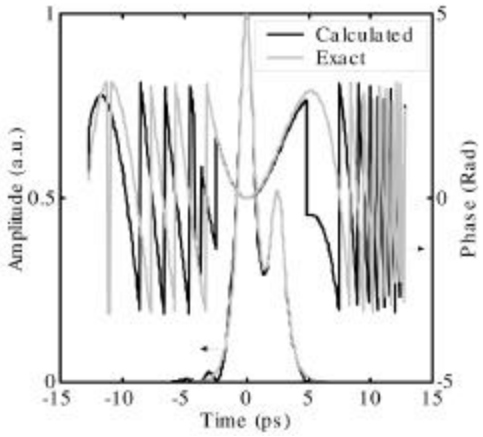

Figure 4: Recovered electric-field of chirped double pulse. Slight ringing artifact on the leading edge of amplitude is mainly due to the finite expansion of 16 Hermite-Gaussian functions. Using more terms would reconstruct that part better.

In conclusion, we have demonstrated the use of a genetic algorithm to recover the amplitude and chirp from a series of autocorrelation measurements after propagation through different spans of fiber. The strength of the genetic algorithm is the ease in which it deals with nonlinearities in the fiber. We have also shown that it is capable of recovering complicated pulse shapes, such as a chirped double pulse with noisy autocorrelations. In addition, the computation speed of the genetic algorithm was greatly enhanced by using Hermite-Gaussian coefficients and chirp coefficients for the genes, which effectively filtered the search space and reduced its dimensionality.

References

1. J.-C. M. Diels, J. J. Fontaine, I. C. McMichael, and F. Simoni, “Control and measurements of ultrashort pulse shapes (in amplitude and phase) with femtosecond accuracy,” *Applied Optics* 24:1270-1282 (1985).

2. R. G. M. P. Koumans and A. Yariv, “Time-resolved optical gating based on dispersive propagation: a new method to characterize optical pulses,” *IEEE Journal of Quantum Electronics* 36:137-144 (2000).

3. J. W. Nicholson, F. G. Omenetto, D. J. Funk, and A. J. Taylor, “Evolving FROGS: phase retrieval from frequency-resolved optical gating measurements by use of genetic algorithms,” *Optics Letters* 24: 490-492 (1999).

4. R. Trebino and D. J. Kane, “Using phase retrieval to measure the intensity and phase of ultrashort pulses -- frequency resolved optical gating,” *Journal of the Optical Society of America A* 10:1101-1111 (1993).

Publications

1. L. A. Jiang, M. E. Grein, and E. P. Ippen, "Frequency resolved optical gating pulse retrieval using using genetic algorithm with Hermite-Gaussian expansion," submitted to *IEEE Journal of Quantum Electronics.*

2. L. A. Jiang, M. E. Grein, and E. P. Ippen, "Full-pulse characterization using autocorrelations and genetic algorithm," submitted to the *Journal of the Optical Society of America B.*

9. Ultrafast recovery times in implanted semiconductor saturable absorber mirrors for 1.5 ?m wavelengths

Sponsor:

AFOSR, DARPA

Project Staff:

J. T. Gopinath, Dr. E. R. Thoen, Dr. E. M. Koontz, Dr. J. P. Donnelly, M. E. Grein, Professor L. A. Kolodziejski, and Professor E. P. Ippen

Semiconductor saturable absorbers have important applications in optical switching and mode-locked lasers. Materials with relatively short recovery times, which maintain large nonlinearities and low non-saturable losses, are required for these applications. Thus, for fast devices, lifetime reduction techniques, such as low-temperature (LT) growth or ion bombardment, are necessary. To assess the effects of the latter, we have recently carried out a detailed study of the effects of proton bombardment on InGaAs/InP saturable absorber mirrors. The device investigated was an antireflection-coated ?/2 InP layer, containing six centered InGaAs quantum wells (? ~1.58 ?m), deposited on a 22 period GaAs/AlAs distributed Bragg reflector. Devices were studied with a collinear degenerate cross-polarized pump-probe technique, using 150 fs pulses from an optical parametric oscillator at 1.54 ?m. Carrier dynamics are comparable to those observed in similar structures [1] [2]. At fluences below complete absorption saturation, state filling produces bleaching of the absorption. Above these fluences, two-photon absorption (TPA) and TPA-induced free-carrier absorption (FCA) occur.

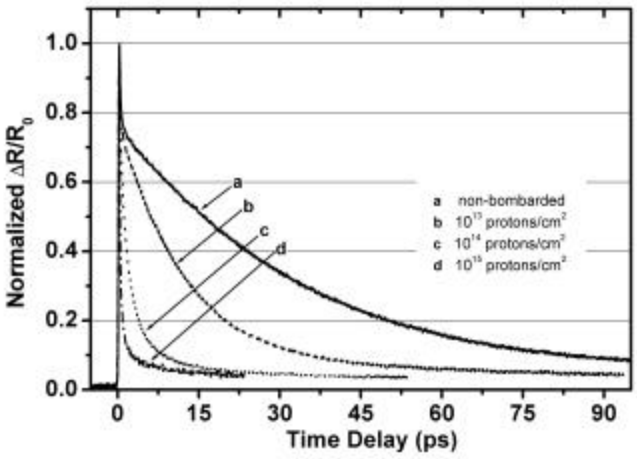

Figure 1: Differential reflectivity measurements as a function of bombardment at 1.54 ?m and a fluence of ~44 ?J/cm^2.

For low optical fluences (where bleaching dominates rather than TPA and FCA), lifetimes are reduced in proton-bombarded structures to ~1 ps, without a significant decrease in modulation depth or increase in the non-saturable loss. Lifetimes of 2.5 ps have been observed in LT InGaAs [3], and 1.7 ps in O+ or Ni+ implanted InGaAs [4]. Figure 1 shows a comparison at low fluence of a non-bombarded structure and structures bombarded with 40 keV protons of differing doses. The observed lifetimes are respectively: non-bombarded ~40 ps; 10^{13} protons/cm^2 ~12 ps, 10^{14} protons/cm^2 ~3 ps, and 10^{15} protons/cm^2 ~1ps. The decrease in lifetime is also accompanied by a small increase in non-saturable loss (an increase of a few percent) and a slight decrease in modulation depth, consistent with observations in LT GaAs [5]. These undesirable effects were mitigated with a rapid (20 s) anneal.

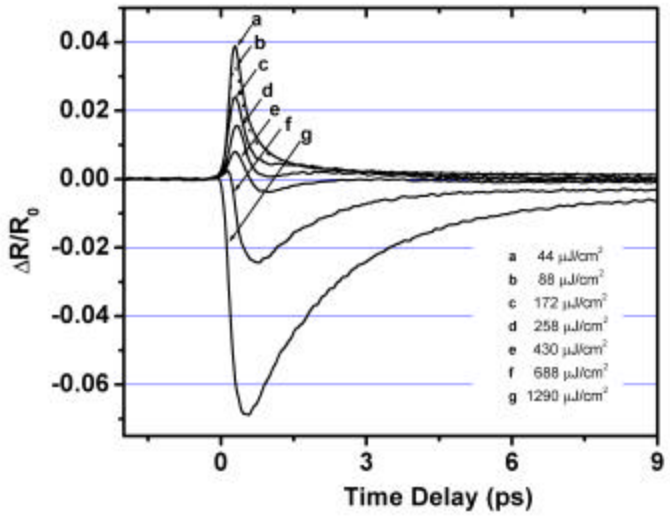

Figure 2: Differential reflectivity measurements as a function of excitation fluence at 1.54 ?m. The sample was bombarded with 40 keV protons, at a dosage of 10^{15} protons/cm^2.

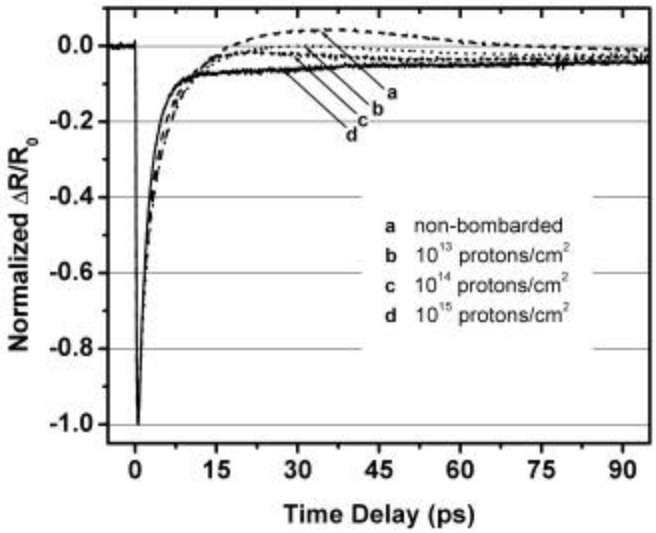

Figure 3: Differential reflectivity measurements as a function of bombardment at 1.54 ?m and a fluence of ~1290?J/cm^2.

The fluence-dependent dynamics for a 10^{15} protons/cm^2 absorber are shown in Figure 2. At low fluences (Figure 2, 44 ?J/cm^2), a ~1 ps response time is apparent. However, as the fluence is increased to levels where significant induced absorption is apparent (Figure 2, 688, 1290 ?J/cm^2), it is clear that the device response time is limited by the non-equilibrium absorption dynamics. This regime is important for applications requiring intensity limiting. Previous work [2] has indicated that the extended relaxation of the induced absorption could be due to carrier capture outside the InGaAs quantum wells, carriers trapped in satellite valleys, or phonon bottleneck effects. A comparison between non-bombarded and bombarded samples at 1290 ?J/cm^2 is shown in Figure 3. In contrast to the recombination (interband process), the relaxation of the excited state intraband absorption is not as affected by the bombardment. Saturation of defect states can also reduce the effectiveness of bombardment.

Sub-picosecond pulses were obtained when the bombarded samples were used to mode-lock a linear erbium-doped soliton fiber laser. No significant threshold differences were observed, validating the small non-saturable loss increase with bombardment.

References

1. P. Langlois, M. Joschko, E. R. Thoen, E. M. Koontz, F. X. Kärtner, E. P. Ippen, and L. A. Kolodziejski, "High fluence ultrafast dynamics of semiconductor saturable absorber mirrors," *Appl. Phys. Lett*. 75: 3841 (1999).
2. M. Joschko, P. Langlois, E. R. Thoen, E. M. Koontz, E. P. Ippen, and L. A. Kolodziejski, "Ultrafast hot-carrier dynamics in semiconductor saturable absorbers," *Appl. Phys. Lett*. 76: 1383 (2000).
3. S. Gupta, J. F. Whitaker, and G. A. Mourou, "Ultrafast carrier dynamics in III-V semiconductors grown by molecular-beam epitaxy at very low substrate temperatures," *IEEE J. Quant. Elect.* 28: 2464-2472 (1992).
4. E. L. Delpon, J. L. Oudar, N. Bouché, R. Raj, A. Shen, N. Stelmakh, and J. M. Lourtioz, "Ultrafast excitonic saturable absorption in ion-implanted InGaAs/InAlAs multiple quantum wells," *App. Phys. Lett.* 72: 759-761 (1998).
5. M. Haiml, U. Siegner, F. Morier-Genoud, U. Keller, M. Luysberg, R. C. Lutz, P. Specht, and E. R. Weber, "Optical nonlinearity in low-temperature-grown GaAs: microscopic limitations and optimization strategies," *App. Phys. Lett.* 74: 3134-3136 (1999).

Publications

1. J. T. Gopinath, E. R. Thoen, E. M. Koontz, M. E. Grein, L. A. Kolodziejski, E. P. Ippen, and J. P. Donnelly, "Ultrafast recovery times in implanted semiconductor saturable absorber mirrors at 1.5 ?m." To be presented at the 2001 Conference on Lasers and Electro-Optics, Baltimore, Maryland, May 6-11, 2001.

2. J. T. Gopinath, E. R. Thoen, E. M. Koontz, M. E. Grein, L. A. Kolodziejski, E. P. Ippen, and J. P. Donnelly, "Recovery Dynamics in Proton-Bombarded Semiconductor Saturable Absorber Mirrors." *Appl. Phys. Lett*. Forthcoming.

10. Enhanced Light Extraction from a Two-Dimensional Photonic Bandgap Light-Emitting Diode

Sponsors

NSF-MRSEC, AFOSR

Project Staff

Daniel Ripin, Alexei Erchak, Dr. Shanhui Fan, Peter Rakich, Dr. Gale Petrich, Professor Erich P. Ippen, Professor John D. Joannopoulos, Professor Leslie A. Kolodziejski

Semiconductor light-emitting diodes (LEDs) are used in a variety of displays, indicators, lighting applications, and even short distance communication systems. They are popular because of the high brightness, low power consumption, and long lifetime. Depending on the geometry of a particular structure, semiconductor LEDs can be plagued by low efficiencies due to poor light extraction. In a typical structure, only 2.5% of the light generated will be extracted out of the device's top surface, while the rest is trapped by guided modes in the high-index semiconductor material.

Photonic crystals, materials with a spatially periodic refractive index, can be designed to efficiently couple light from the dielectric guided modes into free space. [1] In particular, two-dimensional photonic crystals with the proper dimensions can coherently couple light from waveguide modes into highly directional radiation modes by Bragg scattering. To demonstrate this effect we have fabricated a InGaP/InGaAs quantum well LED, with emission centered around 980 nm. A two-dimensional photonic crystal microstructure is then fabricated within the LED by electron beam lithography, and is designed to inhibit waveguide modes at the emission frequency. Surface normal photoluminescence (PL) is observed to increase by as much as a factor of 8 in the photonic crystal region compared to regions on the same LED structure without photonic crystals.

The two-dimensional photonic crystal LED consists of an InGaP/InGaAs active quantum well region, a low refractive index Al_xO_y spacer layer, and an Al_xO_y/GaAs distributed Bragg reflector (DBR) with a calculated stop band from 800 nm to 1400 nm. The structure is fabricated using gas source molecular beam epitaxy, direct-write electron beam lithography, reactive-ion etching, and oxidation processes. [2] The two-dimensional photonic crystal consists of a triangular lattice of holes etched within the upper InGaP cladding layer, with a nominal hole-to-hole spacing of 315 nm and a nominal hole diameter of 220 nm. The holes do not penetrate into the InGaAs quantum well layer, to avoid creating additional non-radiative surface recombination. Each two-dimensional photonic crystal LED is a 30 ?m by 30 ?m region within a 50 ?m by 50 ?m LED mesa. Structure schematics and scanning electron micrographs of a structure are shown in Fig. 1.

Room temperature PL spectroscopy is performed with a cw 810 nm Ti:Al_2O_3 pump laser focused by a microscope objective onto the LED sample. The pump is absorbed by the InGaAs quantum well layer but prevented from reaching the GaAs substrate by the underlying DBR. The PL is collected by the same microscope objective and spectrally resolved by an optical spectrum analyzer or imaged onto a Si CCD camera. At room temperature, the LEDs emit light centered at 980 nm with a full width at half maximum of ~ 60 nm.

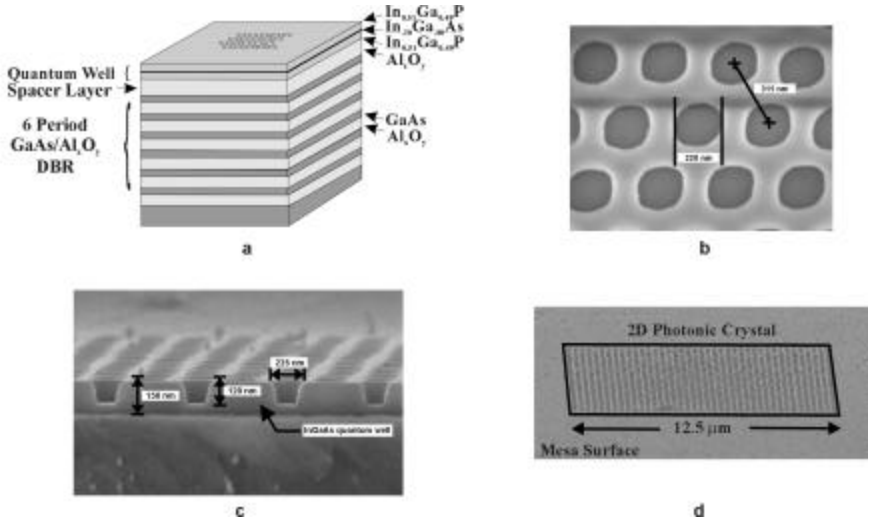

Figure 1: a) Schematic of a InGaP/InGaAs2-D PBG LED structure. b) A scanning electron micrograph (SEM) of the triangular lattice of holes forming the photonic crystal. c) Cross sectional SEM of 2-D PBG LED structure. d) SEM of the entire 2-D photonic crystal array.

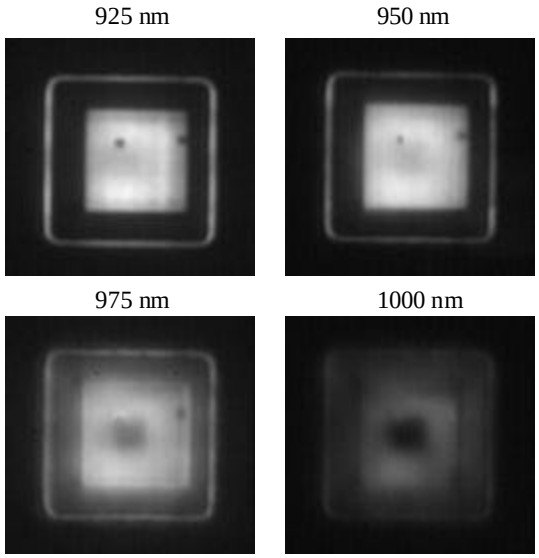

Figure 2: Si CCD images of a photonic crystal LED mesa. The images are taken with a 10 nm FWHM filter centered at 925 nm, 950 nm, 975 nm, and 1000 nm. A strong enhancement in the central photonic crystal region as compared with the unpatterned border region is visible at 925 nm and 950 nm.

CCD images of a LED mesa containing a photonic crystal optimized for scattering light at 925 nm are shown in Figure 2. The LED mesa was pumped by a 75 ?m spot size. Each image is recorded with a chromatic filter of 10 nm full width at half maximum centered at 925 nm, 950 nm, 975 nm, and 1000 nm respectively. In the images, it is possible to directly compare the intensity of light coming from the 30 ?m by 30 ?m photonic crystal region in the center of the mesa to the unpatterned border region of the 50 ?m by 50 ?m LED mesa. Strong enhancements at 925 nm and 950 nm are visible compared with similar images at 975 nm and 1000 nm.

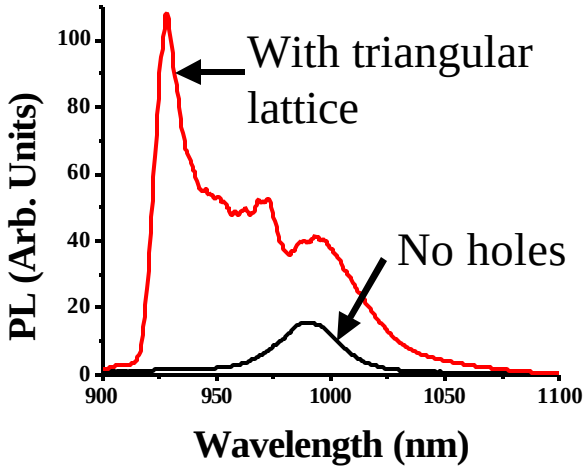

Fig. 3. Photoluminescence spectra of a photonic crystal LED and an unpatterned LED. The photonic crystal LED has a large enhancement of the PL centered at 925 nm.

A complete spectrum of the PL for an LED with and without photonic crystal patterning is shown in Figure 3. The collected PL is dramatically higher for the photonic crystal LED. Furthermore, the spectral lineshape is significantly altered and shows a strong peak at 925 nm corresponding to resonance with a Bragg scattering state. Integrated over all wavelengths, 8 times more PL was collected for the photonic crystal LED compared with an unpatterned LED. At 925 nm, 100 times more PL was recorded. The Bragg scattering is so effective because it directionally couples light from the guided modes of the LED structure into free-space modes propagating normally to the LED surface. This light is easily collected by the experimental apparatus.

References

1. Alexei A. Erchak, Daniel J. Ripin, Shanhui Fan, Peter Rakich, John D. Joannopoulos, Erich P. Ippen, Gale S. Petrich and Leslie A. Kolodziejski, "Enhanced coupling to vertical radiation using a two-dimensional photonic crystal in a semiconductor light-emitting diode," *APL* 78: 563-565 (2001).

2. See RLE Progress Report 2000 of Professor Leslie A. Kolodziejski.

11. Near-Field Optical Characterization of Two-Dimensional Photonic Bandgap Crystals

Sponsors

NSF-MRSEC

Project Staff

Peter Rakich, Daniel Ripin, Alexei Erchak, Shanhui Fan, Dr. Gale Petrich, Professor Erich P. Ippen, Professor John D. Joannopoulos, Professor Leslie A. Kolodziejski

Near-field scanning optical microscopy (NSOM) is a technique whereby sub-wavelength images (~?/20 resolution) can be acquired by scanning a small aperture, such as that formed at the end of a tapered fiber, very close to the specimen of interest. With the continually decreasing size of micro-photonic devices, conventional far-field methods no longer have the resolution to

characterize the optical fields inside of these structures. Especially for high-index micro-photonic devices such as waveguides and photonic bandgap crystals, NSOM may prove to be the dynamic tool needed.

Measurements of the internal spatial modes of many photonic devices may be performed through a near-field photon-tunneling method, which exploits frustrated total internal reflection (FTIR). If a tapered fiber is brought in very close proximity (~10-30 nm) to the waveguide, a small fraction of the guided light may "tunnel" into the tapered fiber, allowing the experimenter to measure the spatial light intensity at that point in the waveguide. Similarly, one could use this technique to determine the internal spatial modes of two-dimensional photonic bandgap crystals, which have been fabricated on planar waveguide structures.

A thorough computational study of this type of FTIR near-field characterization method has been performed by S. Fan and J. D. Joannopoulos [1]. A complete three-dimensional finite-difference time domain simulation was performed to determine the coupling efficiencies and spatial resolution achievable with high-index photonic bandgap specimens such as those described in ref. [3]. This study clearly indicates that, under realistic experimental conditions, near-field measurements will allow the experimenter to completely map out the entire band structure of these two-dimensional photonic bandgap crystals.

Measurements are currently under way for the characterization of the internal spatial modes of a two-dimensional photonic bandgap LED. The photonic crystal LED under measurement consists of an InGaP/InGaAs active quantum well region, beneath which is a low refractive index Al_xO_y spacer layer and an Al_xO_y/GaAs distributed Bragg reflector (DBR) having a band stop from 800 to 1400 nm. This structure, alone, acts as a planar waveguide, which captures and guides most of the photoluminescent light. However, in the middle of these planar LED structures a periodic lattice of holes has been etched so as to form a photonic bandgap crystal, which prevents certain wavelengths from propagating in the LED. Structure schematics and scanning electron micrographs of the LEDs under study see ref. [3].

In these experiments we excite a photoluminescent InGaAs quantum well with a short wavelength pump (either argon or Ti:Sa) which is focused through a microscope objective. Much of the spontaneous emission, which results from the relaxation of the quantum well states, is coupled into guided modes. When the guided radiation enters the photonic crystal region it excites distinct spatial light modes, some propagating and some not. The spatial character of each of these modes may be measured by collecting the photoluminescent light through a fiber probe, which is in close proximity to the LED surface. To demonstrate that our current near-field apparatus is capable of sub-wavelength resolution, we have passed light through the fiber tip which was scanned in close proximity to the LED surface. Modulation of the scattered light results in a sub-wavelength image of the photonic crystal. A comparison of this near-field image with a SEM image is made in Fig. 1.

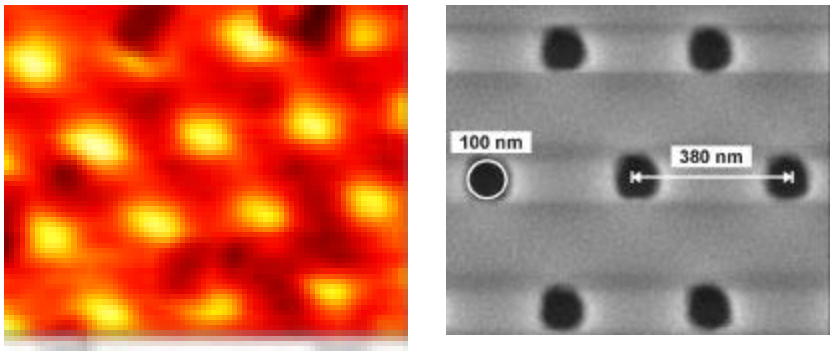

a b

Figure 1: a) Subwavelength near-field image of PBG LED taken in oblique reflection/collection geometry. b) The corresponding SEM image of the same sample. The hexagonal lattice formed by the holes can be clearly seen.

References

1. Shanhui Fan, Ian Appelbaum, and J. D. Joannopoulos, "Near-field scanning optical microscopy as a simultaneous probe of fields and band structure of photonic crystals: A computational study," *Appl. Phys. Lett.* 75: 3461-3463, (1999)

2. Alexei A. Erchak, Daniel J. Ripin, Shanhui Fan, Peter Rakich, John D. Joannopoulos, Erich P. Ippen, Gale S. Petrich and Leslie A. Kolodziejski, "Enhanced coupling to vertical radiation using a two-dimensional photonic crystal in a semiconductor light-emitting diode," *Appl. Phys. Lett.* 78: 563-565 (2001).

3. See Figure 1 of report above on: Enhanced Light Extraction from a Two-Dimensional Photonic Bandgap Light-Emitting Diode